An Azimuth-Dependent Phase Gradient Autofocus (APGA) Algorithm for Airborne/Stationary BiSAR Imagery

Song Zhou, Mengdao Xing, *Member, IEEE*, Xiang-Gen Xia, *Fellow, IEEE*, Yachao Li, Lei Zhang, and Zheng Bao, *Senior Member, IEEE*

***Abstract*—In airborne/stationary bistatic-synthetic-aperture-radar imaging, translational invariance was no longer valid. After range cell migration correction, the range-compressed signal under the same range gate exhibited azimuth-dependent FM rates that made the motion-induced phase error difficult to separate from the echoes. To solve this problem, an azimuth-dependent phase gradient autofocus (PGA) algorithm was proposed. Different from the conventional PGA, the residual quadratic phase arising from the azimuth-dependent FM rates was additionally estimated and compensated. As the influence of the azimuth-dependent FM rates was greatly reduced, a phase gradient estimator was subsequently applied for accurate phase error retrieval. Acquired raw data were analyzed to verify the proposed algorithm.**

***Index Terms*—Airborne/stationary (A/S) configuration, azimuth-dependent phase gradient autofocus (PGA) (APGA) algorithm, bistatic synthetic aperture radar (SAR) (BiSAR), residual quadratic phase (RQP).**

I. Introduction

AMONG the various configurations of bistatic synthetic aperture radar (SAR) (BiSAR), the airborne/stationary (A/S) BiSAR (A/S-BiSAR) case is relatively easy to be realized, and the motion compensation (MOCO) only needs to be considered for the airborne platform. For the MOCO problem, the phase gradient autofocus (PGA) algorithm is well known, which is able to estimate and correct the motion-induced phase error within an accuracy level at subradian [1]–[3]. In A/S-BiSAR, however, as the relative positions of the transmitter and the receiver change with time, the echoes of the scatterers with the identical minimal bistatic range exhibit azimuth-dependent FM rates [4], [5]. Thus, if the PGA is directly applied, the influence of the azimuth-dependent FM rates will be involved in the phase error estimation that can then prevent the accurate compensation of the phase error.

To deal with this problem, the PGA algorithm is modified. Different from the PGA, the azimuth positions of the sampled scatterers are extracted from the echoes in the azimuth-frequency domain. According to these azimuth positions, the residual quadratic phase (RQP) arising from the azimuth-dependent FM rates is additionally estimated and compensated for each sample. After the influence of the azimuth-dependent FM rates is greatly reduced, the phase error is accurately retrieved by applying a phase gradient estimator to the RQP-compensated echoes. Since the RQP estimation and compensation depend on the azimuth positions of the sampled scatterers, we name this proposed solution as the azimuth-dependent PGA (APGA) algorithm. Analyses of acquired raw data show that the performance of the APGA is superior to that of the conventional PGA in the A/S-BiSAR application. Details are given in the following sections.

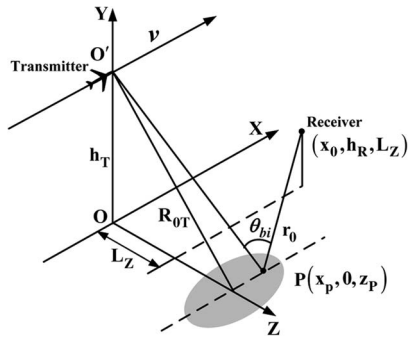

Fig. 1. A/S-BiSAR geometry.

II. A/S-BiSAR Geometry and Signal Model

The A/S-BiSAR geometry is shown in Fig. 1. The transmitter is mounted on an aircraft as the illuminator. The receiver is fixed on a hill near the scenario. The moving transmitter operates in the strip-map mode with a zero squint angle, and the receiver is fixed at (x_0, h_R, L_Z). The transmitter moves along the X-axis with a velocity at v and at a flight height[1] of h_T. Let η denote the azimuth time. At time $\eta = 0$, the antenna phase center of the moving transmitter is at the position O', and the projection of O' on the XOZ plane is the origin of O. θ_{bi} is referred to as the bistatic angle. Assume that the transmitted signal is of a chirp form

$$s_T(\tau) = w_r(\tau)\exp(\mathrm{j}\pi\gamma\tau^2 + \mathrm{j}2\pi f_0\tau) \tag{1}$$

where τ is the range time, γ is the FM rate of the transmitted signal, f_0 is the carrier frequency, and $w_r(\tau)$ is the range

Manuscript received May 7, 2012; revised November 11, 2012; accepted December 18, 2012. Date of publication February 26, 2013; date of current version October 10, 2013. This work was supported in part by the National Natural Science Foundation of China under Grant 61001211 and in part by the Air Force Office of Scientific Research under Grant FA9550-12-1-0055.

S. Zhou is with School of Information Engineering, East China of Jiaotong University, Nanchang, China and also with the National Key Laboratory of Radar Signal Processing, Xidian University, Xi'an 710071, China (e-mail: zhousong8411@sina.com).

M. Xing, Y. Li, L. Zhang, and Z. Bao are with the National Key Laboratory of Radar Signal Processing, Xidian University, Xi'an 710071, China.

X.-G. Xia is with the Department of Electrical and Computer Engineering, University of Delaware, Newark, DE 19716 USA.

Digital Object Identifier 10.1109/LGRS.2013.2237749

[1]The "height" in this letter refers to the height above the land level rather than above the sea level.

envelope. Then, the downconverted echoes from an arbitrary scatterer $P(x_p, 0, z_p)$ can be written as

$$s(\tau,\eta) = \sigma w_r\left[\tau - \frac{R_\Sigma(\eta)+\Delta R(\eta)}{c}\right] w_a\left(\eta - \frac{x_p}{v}\right) \times \exp\left\{\mathrm{j}\pi\gamma\left[\tau - \frac{R_\Sigma(\eta)+\Delta R(\eta)}{c}\right]^2\right\} \times \exp\left[-\mathrm{j}2\pi\frac{R_\Sigma(\eta)+\Delta R(\eta)}{\lambda}\right] \quad (2)$$

where σ is the scattering amplitude, c is the speed of light, $w_a(\eta)$ is the azimuth envelope, and $\lambda = c/f_0$ is the wavelength. $\Delta R(\eta)$ is the motion error caused by the deviation of the real trajectory from the ideal case. $R_\Sigma(\eta)$ is the bistatic range history in the ideal case, and it has

$$R_\Sigma(\eta) = \sqrt{R_{0T}^2 + (v\eta - x_p)^2} + r_0 \quad (3)$$

where $R_{0T} = \sqrt{h_T^2 + z_p^2}$ is the closest slant range from P to the moving transmitter and r_0 is the slant range from P to the stationary receiver.

To reduce the influence of $\Delta R(\eta)$ in the focus of A/S-BiSAR data, the initial MOCO by using the information of the inertial navigation unit (INU)/Global Positioning System (GPS) unit is performed, and the bulk of $\Delta R(\eta)$ can be compensated. After the INU/GPS-based MOCO, only the residual motion error needs to be considered. Let $\Delta R_{res}(\eta)$ denote the error. Generally, for the SAR systems with medium spatial resolution, the influence of $\Delta R_{res}(\eta)$ to the range cell migrations (RCMs) is negligible, but the influence of $\Delta R_{res}(\eta)$ to the azimuth phase merits concern [6]. Therefore, we focus on the range-compressed echoes. After the INU/GPS-based MOCO and the RCM correction (RCMC), the range-compressed echoes of the scatterers are mainly confined in the range gate, $R_{0T} + r_0$ [4], [5]. Let $R_{0\Sigma} = R_{0T} + r_0$, where $R_{0\Sigma}$ is referred to as the minimal bistatic range. Then, by using the Fresnel approximation, the range-compressed echoes can be written as

$$s_{rc}(\tau,\eta) \approx \sigma\mathrm{sinc}\left[B\left(\tau - \frac{R_{0\Sigma}}{c}\right)\right] w_a\left(\eta - \frac{x_p}{v}\right) \times \exp\left[\mathrm{j}\pi K_a \times \left(\eta - \frac{x_p}{v}\right)^2\right] \times \exp\left[-\mathrm{j}\frac{2\pi}{\lambda}\Delta R_{res}(\eta)\right] \quad (4)$$

where B is the bandwidth of the transmitted signal and K_a is the azimuth FM rate. Since $\Delta R_{res}(\eta)$ can still degrade the quality of the final image in focus, data-driven autofocusing techniques (e.g., PGA) are necessary [7].

III. APGA Algorithm

A. A/S-BiSAR Signal Properties

Prior to the presentation of the proposed algorithm, signal properties of the A/S-BiSAR need to be analyzed. So as to apply the PGA in the strip-map SAR autofocusing, an effective approach is to divide the strip-map SAR data into small subaperture data blocks. Then, the subaperture echoes can be converted into spotlight form by using an azimuth-deramping operation, and the PGA is subsequently employed [8]. Similar

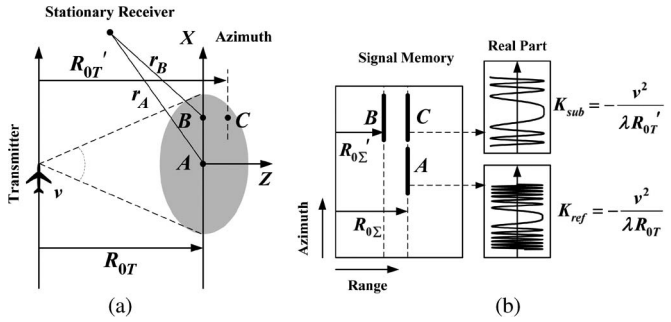

Fig. 2. Origin of the azimuth-dependent FM rates in the A/S-BiSAR processing. (a) A/S-BiSAR geometry and three scatterers are considered. (b) Range-compressed echoes in the signal memory.

to (4), the subaperture echoes (before azimuth-deramping operation) can be written as

$$s_{rc\_sub}(\tau,\eta) \approx \sigma\mathrm{sinc}\left[B\left(\tau - \frac{R_{0\Sigma}}{c}\right)\right] w_a\left(\eta - \frac{x_p}{v}\right) \times \exp\left[\mathrm{j}\pi K_{sub}(R_{0\Sigma},\Delta x_p) \times \left(\eta - \frac{x_p}{v}\right)^2\right] \times \exp\left[-\mathrm{j}\frac{2\pi}{\lambda}\Delta R_{res\_sub}(\eta)\right] \quad (5)$$

where $\Delta R_{res\_sub}(\eta)$ is the residual motion error of the subaperture. Δx_p is the offset of the scatterer relative to x_{ref}, and x_{ref} is the middle azimuth position of the subaperture. For a scatterer at x_p, it has $x_p = x_{ref} + \Delta x_p$. $K_{sub}(R_{0\Sigma}, \Delta x_p)$ is the azimuth FM rate of the subaperture. In A/S-BiSAR, it is known that the azimuth FM rates of the echoes under a same range gate are related to the azimuth positions of the scatterers [4], [5], and $K_{sub}(R_{0\Sigma}, \Delta x_p)$ can be approximated by

$$K_{sub}(R_{0\Sigma},\Delta x_p) \approx K_{ref}(R_{0\Sigma}, x_{ref}) - p_1\frac{\Delta x_p}{v} - p_2\left(\frac{\Delta x_p}{v}\right)^2 \quad (6)$$

where $K_{ref}(R_{0\Sigma}, x_{ref})$ is the azimuth FM rate of the scatterers at x_{ref} and $K_{ref}(R_{0\Sigma}, x_{ref})$ is referred to as the reference azimuth FM rate. p_1 and p_2 are the perturbation coefficients.

Fig. 2 explains the origin of the azimuth-dependence of $K_{sub}(R_{0\Sigma}, \Delta x_p)$ (without considering the motion error). Owing to the A/S-BiSAR configuration with stationary receiver, after RCMC, the range compressed echoes of A and C have been "pulled" into the same range gate $R_{0\Sigma}$. Since their $R_{0T} \neq R'_{0T}$, the azimuth FM rates of A and C are different. In the following sections, the influence of the azimuth-dependent $K_{sub}(R_{0\Sigma}, \Delta x_p)$ to the phase error estimation will be discussed in detail and a modified PGA algorithm will be derived.

B. Influence of Azimuth-Dependent FM Rates

To facilitate the discussion of the influence of the azimuth dependence of $K_{sub}(R_{0\Sigma}, \Delta x_p)$ in the PGA processing, the subaperture data block is then converted into spotlight form by employing an azimuth-deramping operation [8], and the PGA is subsequently applied. Usually, the azimuth-deramping function

follows the middle azimuth position of the subaperture, and it is given by

$$H_{deramp}(\eta; R_{0\Sigma}) = \exp\left[-\mathrm{j}\pi K_{ref}(R_{0\Sigma}, x_{ref}) \times \left(\eta - \frac{x_{ref}}{v}\right)^2\right]. \quad (7)$$

By multiplying (5) with (7), the deramped echoes can be written as

$$s_{deramp}(\tau, \eta) = \sigma \mathrm{sinc}\left[B(\tau - \frac{R_{0\Sigma}}{c})\right] \times \exp\left[\mathrm{j}\varphi_{deramp}(\eta; R_{0\Sigma}, \Delta x_p)\right] \quad (8)$$

where

$$\begin{aligned}\varphi_{deramp}(\eta; R_{0\Sigma}, \Delta x_p) = &-\frac{2\pi}{\lambda}\Delta R_{res\_sub}(\eta) \\ &+ \left[-2\pi K_{ref}(R_{0\Sigma}, x_{ref})\frac{\Delta x_p}{v} \right. \\ &\left. + 2\pi p_1\left(\frac{\Delta x_p}{v}\right)^2 + 2\pi p_2\left(\frac{\Delta x_p}{v}\right)^3\right]\left(\eta - \frac{x_{ref}}{v}\right) \\ &+ \left[\pi K_{ref}(R_{0\Sigma}, x_{ref})\left(\frac{\Delta x_p}{v}\right)^2 \right. \\ &\left. - \pi p_1\left(\frac{\Delta x_p}{v}\right)^3 - \pi p_2\left(\frac{\Delta x_p}{v}\right)^4\right] \\ &+ \varphi_{RQP}(\eta; R_{0\Sigma}, \Delta x_p). \end{aligned} \quad (9)$$

In (9), $\varphi_{deramp}(\eta; R_{0\Sigma}, \Delta x_p)$ consists of four components: The first term $-(2\pi/\lambda)\Delta R_{res\_sub}(\eta)$ indicates the phase error introduced by $\Delta R_{res\_sub}(\eta)$, which should be separated from the echoes for a well-focused SAR image. The second term is linearly related to η. In the PGA processing, the second term can be removed by circularly shifting the samples to the center of the image [1]. The third term is independent of η. Therefore, the second and third terms do not influence the phase gradient estimation for $-(2\pi/\lambda)\Delta R_{res\_sub}(\eta)$ significantly. Let us focus on the fourth term $\varphi_{RQP}(\eta; R_{0\Sigma}, \Delta x_p)$, which is referred to as the RQP term and can be written as

$$\varphi_{RQP}(\eta; R_{0\Sigma}, \Delta x_p) = \left[-\pi p_1\frac{\Delta x_p}{v} - \pi p_2\left(\frac{\Delta x_p}{v}\right)^2\right] \times \left(\eta - \frac{x_{ref}}{v}\right)^2. \quad (10)$$

From the derivations of (7)–(10), it can be seen that the RQP term is arising from the azimuth-dependent $K_{sub}(R_{0\Sigma}, \Delta x_p)$ after the azimuth-deramping operation. Since the RQP term is a quadratic term of η, the gradient of the RQP will be included in the phase gradient estimation if the conventional PGA is directly applied.

The influence of the azimuth-dependent FM rates can be seen in Fig. 3, and the main steps in the focus of A/S-BiSAR data by using the conventional PGA are shown in Fig. 4 (without including the dashed block). The dashed lines in Fig. 3 indicate the phase error contained in the echoes. After the INU/GPS-based MOCO and the RCMC, the range-compressed echoes of three sampled scatterers under the same range gate are investigated, as shown in Fig. 3(a). Assume that scatterer 2 is located at x_{ref}, while scatterers 1 and 3 are away from x_{ref}. Thus, the azimuth FM rates of the scatterers are different

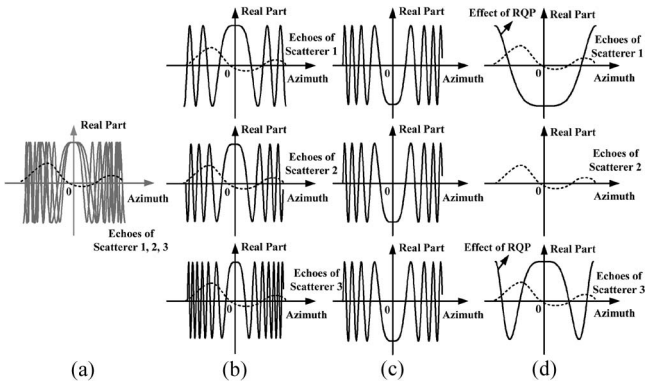

Fig. 3. Influence of the azimuth-dependent FM rates to the phase error estimation. (a) Echoes prior to the azimuth deramping. (b) Echoes of scatterers 1, 2, and 3, which are analyzed independently. (c) Azimuth-deramping function. (d) Echoes after the azimuth deramping.

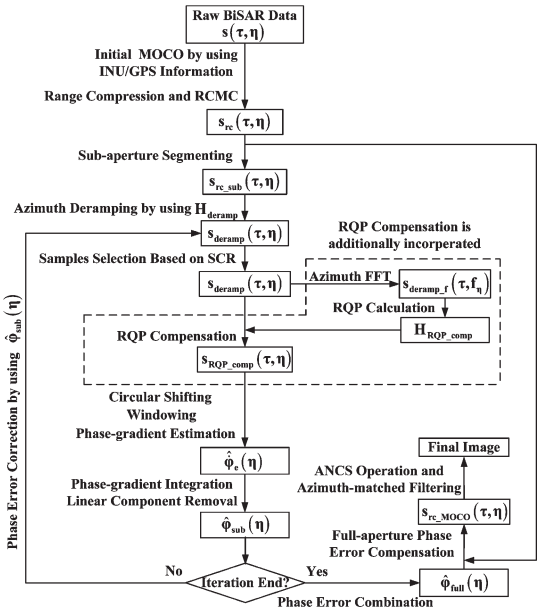

Fig. 4. Main steps in the focus of A/S-BiSAR data by using the conventional PGA (without including the dashed block) and the proposed APGA (including the dashed block).

independently from each other, as analyzed in Fig. 3(b). The azimuth-deramping function is shown in Fig. 3(c), and the deramped echoes are shown in Fig. 3(d). Since the deramping function follows x_{ref}, only the deramped echoes of scatterer 2 do not contain the RQP. As the azimuth FM rate of scatterer 1 (or 3) is different from that of scatterer 2, the RQP is inevitably introduced, as shown in Fig. 3(d). Therefore, when we come to the step of "Samples Selection" in Fig. 4 (the other steps and symbols below "Samples Selection" will be mentioned in Section III-C) and if the deramped echoes of scatterer 1 (or 3) are selected for the phase gradient estimation, the RQP will be treated as a "false" phase error that prevents the "true" phase error from being separated.

Therefore, in the PGA processing, the RQP needs to be compensated prior to the phase gradient estimation.

C. APGA Algorithm

From (10), it can be seen that the RQP is related to the azimuth positions of the sampled scatterers. Thus, for the

compensation of the RQP, the Δx_p of the sampled scatterers should be extracted from the echoes. Thus, we come back to the deramped echoes expressed in (8) and (9). By using an azimuth fast fourier transform (FFT) to (8), the echoes are transformed into the azimuth-frequency domain and can be written as

$$s_{\text{deramp\_f}}(\tau, f_\eta) = \sigma_1 \text{sinc}\left[B\left(\tau - \frac{R_{0\Sigma}}{c}\right)\right] \times G\left[(f_\eta - f_{\eta 0})\right] \quad (11)$$

where σ_1 is the scattering amplitude. $G(f_\eta)$ is the response function, and the shape of $G(f_\eta)$ is related to $-(2\pi/\lambda)\Delta R_{res\_sub}(\eta)$ and $\varphi_{RQP}(\eta; R_{0\Sigma}, \Delta x_p)$. If (9) does not contain $-(2\pi/\lambda)\Delta R_{res\_sub}(\eta)$ and $\varphi_{RQP}(\eta; R_{0\Sigma}, \Delta x_p)$, then $G(f_\eta)$ is sinc(f_η). In (11), $f_{\eta 0}$ can be formulated as

$$f_{\eta 0} = -K_{ref}(R_{0\Sigma}, x_{ref})\frac{\Delta x_p}{v} + p_1\left(\frac{\Delta x_p}{v}\right)^2 + p_2\left(\frac{\Delta x_p}{v}\right)^3 + l_0 \quad (12)$$

where l_0 is from the linear components of $\Delta R_{res\_sub}(\eta)$ with respect to η. As mentioned in Section II, $\Delta R_{res\_sub}(\eta)$ is the residual motion error after the INU/GPS-based MOCO or other coarse MOCO. Thus, for a duration of η, the linear component of $\Delta R_{res\_sub}(\eta)$ is usually very small, and the contribution of l_0 to $f_{\eta 0}$ is negligible. $f_{\eta 0}$ can be approximated by

$$f_{\eta 0} \approx -K_{ref}(R_{0\Sigma}, x_{ref})\frac{\Delta x_p}{v} + p_1\left(\frac{\Delta x_p}{v}\right)^2 + p_2\left(\frac{\Delta x_p}{v}\right)^3. \quad (13)$$

In (13), $f_{\eta 0}$ indicates the locations of $G(f_\eta)$ of the sampled scatterers in the azimuth-frequency domain, from which Δx_p can be estimated. Note that, in (13), the second and third terms are very small compared with the first term. Thus, Δx_p can be estimated by ignoring the contributions of the second and third terms

$$\Delta \hat{x}_p \approx -\frac{v}{K_{ref}(R_{0\Sigma}, x_{ref})} \times f_{\eta 0} \quad (14)$$

where $\Delta \hat{x}_p$ denotes the estimated Δx_p of the sampled scatterers. Here, it should be noticed that the estimated error of $\Delta \hat{x}_p$ may be introduced by the seriously corrupted shape of $G(f_\eta)$. Fortunately, as the phase estimation and correction are repeated iteratively in the PGA processing, the scatterers in the azimuth-frequency domain become more and more focused, and the shape of $G(f_\eta)$ gradually approaches to "sinc" shape; thus, $\Delta \hat{x}_p$ converges to an accurate value. According to (10), the RQP compensation function is then given by

$$H_{RQP\_comp}(\eta; R_{0\Sigma}, \Delta \hat{x}_p) = \exp\left\{\left[\text{j}\pi p_1 \frac{\Delta \hat{x}_p}{v} + \text{j}\pi p_2\left(\frac{\Delta \hat{x}_p}{v}\right)^2\right] \times \left(\eta - \frac{x_{ref}}{v}\right)^2\right\}. \quad (15)$$

By multiplying (8) with (15), the RQP is compensated. The RQP-compensated echoes can be written as

$$s_{RQP\_comp}(\tau, \eta) = \sigma \text{sinc}\left[B\left(\tau - \frac{R_{0\Sigma}}{c}\right)\right] \times \exp\left[\text{j}\varphi_{RQP\_comp}(\eta; R_{0\Sigma}, \Delta x_p)\right] \quad (16)$$

where

$$\varphi_{RQP\_comp}(\eta; R_{0\Sigma}, \Delta x_p) = -\frac{2\pi}{\lambda}\Delta R_{res\_sub}(\eta) + \left[-2\pi K_{ref}(R_{0\Sigma}, x_{ref})\frac{\Delta x_p}{v} + 2\pi p_1\left(\frac{\Delta x_p}{v}\right)^2 + 2\pi p_2\left(\frac{\Delta x_p}{v}\right)^3\right] \times \left(\eta - \frac{x_{ref}}{v}\right) + \left[\pi K_{ref}(R_{0\Sigma}, x_{ref})\left(\frac{\Delta x_p}{v}\right)^2 - \pi p_1\left(\frac{\Delta x_p}{v}\right)^3 - \pi p_2\left(\frac{\Delta x_p}{v}\right)^4\right]. \quad (17)$$

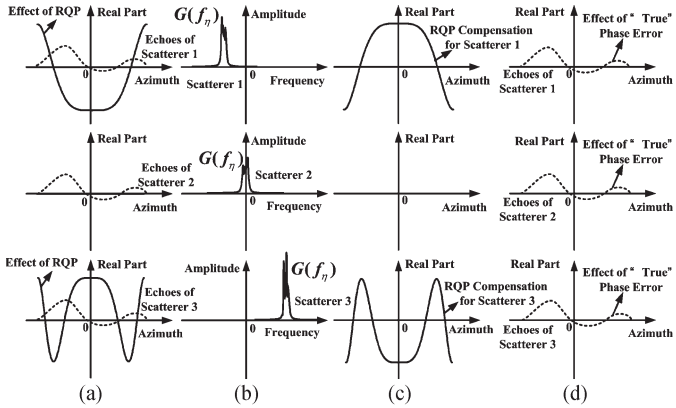

Fig. 5. RQP compensation for the azimuth-deramped echoes. (a) Echoes prior to the RQP compensation. (b) Echoes in the azimuth-frequency domain. (c) RQP compensation functions. (d) RQP is removed, and only the "true" phase error remains.

Comparing (17) with (9), it can be found that the RQP term is finally removed and only three components remain in the RQP-compensated echoes: They are the phase error term $-(2\pi/\lambda)\Delta R_{res\_sub}(\eta)$, the term linearly related to η, and the term independent of η.

The flow diagram of the RQP compensation is shown in Fig. 5, in which the RQP and the phase error are of the primary concerns. By using an azimuth FFT, the echoes are transformed into the azimuth-frequency domain where the scatterers are preliminarily focused around $f_{\eta 0}$, as shown in Fig. 5(b). With $f_{\eta 0}$, Δx_p is estimated, and the RQP compensation function is obtained [see Fig. 5(c)]. After the RQP compensation, the RQP has been removed, and only the "true" phase error remains in the echoes, as shown in Fig. 5(d); a phase gradient estimator is finally applied to the RQP-compensated echoes for accurate phase error retrieval.

The main steps in the focus of A/S-BiSAR data by using the proposed algorithm are shown in Fig. 4 (including the dashed block), and we can see that the steps of the RQP compensation are additionally incorporated. Since the RQP estimation and compensation depend on the azimuth positions of the sampled scatterers, we name this modified PGA algorithm as the APGA algorithm. In Fig. 4, $\hat{\dot{\phi}}_e(\eta)$ denotes the estimated gradient of the phase error. $\hat{\phi}_{sub}(\eta)$ denotes the phase error function obtained by integrating $\hat{\dot{\phi}}_e(\eta)$ and removing its linear component. $\hat{\phi}_{full}(\eta)$ is the full-aperture phase error function obtained by the combination of $\hat{\phi}_{sub}(\eta)$ of each subaperture. $s_{rc\_MOCO}(\tau, \eta)$ denotes the echoes after the full-aperture phase error compensation. In the step of "Samples Selection," the samples with high signal-to-clutter ratio (SCR) are selected,

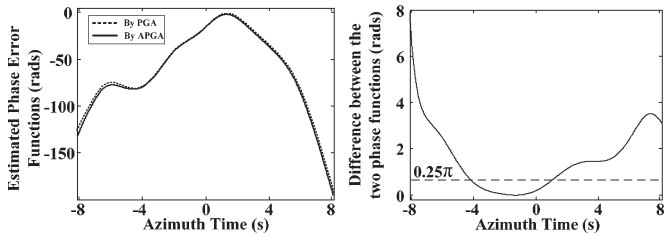

Fig. 6. Full-aperture phase error functions. (a) From both the conventional PGA and the APGA. (b) Differences between the two phase error functions.

which makes the estimation more efficient and accurate [9]. The steps of "Circular Shifting," "Windowing," "Phase-gradient Estimation," "Phase-gradiant Integration," and "Iteration" in Fig. 4 are common to those implemented in the conventional PGA [1]. As the full-aperture phase error is retrieved from the echoes, the azimuth nonlinear chirp scaling (ANCS) algorithm is employed to equalize the azimuth-dependent FM rates for each range bin [4], [5]. Then, the azimuth-matched filtering is applied to obtain a well-focused image.

IV. Analysis of Acquired Raw Data

In the experiment, the receiver is fixed on a hill with a height of 309 m, and the transmitter is mounted on an aircraft with a flight height of 1204 m. The transmitter operates in the stripmap mode with a zero squint angle. The velocity of the moving transmitter is about 64.7 m/s. The transmitter range R_{0T} is about 4500 m, and the bistatic range R_{Σ} is about 7800 m. θ_{bi} is about 12°. The Ku-band transmitted signal is a chirp with a bandwidth of 80 MHz and a duration of 10 μs. The A/D sample rate is 100 MHz, and the pulse repetition frequency is 500 Hz.

In the focus of the full-aperture A/S-BiSAR data, the range-Doppler algorithm is adopted for RCMC, and Hamming windows are used in both the range and the azimuth processing for sidelobe suppressions. In the APGA processing, the length of the azimuth data block is chosen to be 97 m, and 50% overlapping is used in the subaperture segmentations. The analyses of the full-aperture phase error functions are shown in Fig. 6. In Fig. 6(a), the dashed curve denotes the full-aperture phase error function from the conventional PGA, and the solid curve denotes the one from the APGA. The estimated noise is removed by using the polynomial filtering method. The differences between the two functions are shown in Fig. 6(b). It can be seen that the maximum of the differences greatly exceeds the acceptable level 0.25π, which would adversely affect the quality of the final image in focus.

The full-aperture focused image (1.20 × 1.05 km, range × azimuth) obtained from the APGA is shown in Fig. 7. Comparing with the result from the conventional PGA, the entropy of the image decreases from 15.961 to 15.950. The azimuth responses of two prominent scatterers (marked by A and B) are investigated, as shown in Fig. 8. It can be found that the quality of the focused scatterers is effectively improved, which confirms the better performance of the proposed algorithm.

V. Conclusion

In this letter, the signal model of A/S-BiSAR with residual motion error has been analyzed. Due to the azimuth-dependent FM rates, the motion-induced phase error was difficult to separate from the echoes. To solve this problem, a modified PGA algorithm, named APGA, has been proposed. In the APGA, the RQP compensation was additionally incorporated into the conventional PGA processing to reduce the influence of the azimuth-dependent FM rates. Then, the phase gradient estimator was able to be applied to the RQP-compensated echoes for accurate phase error retrieval. Results from the analyses of acquired raw data were promising, and it showed that there was a significant improvement in azimuth focusing as compared to the focused image using the conventional PGA algorithm.

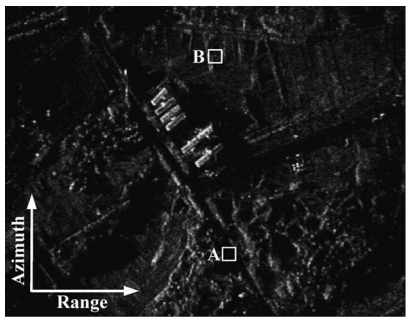

Fig. 7. Full-aperture focused image obtained from the APGA.

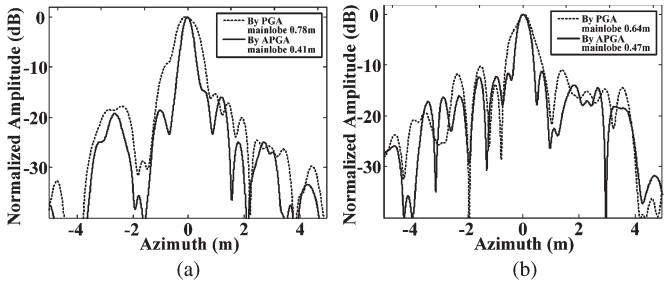

Fig. 8. Azimuth responses of the focused scatterers. (a) Scatterer A. (b) Scatterer B.

References

[1] D. E. Wahl, P. H. Eichel, D. C. Ghiglia, and C. V. Jakowatz, Jr., "Phase gradient autofocus—A robust tool for high resolution phase correction," *IEEE Trans. Aerosp. Electron. Syst.*, vol. 30, no. 3, pp. 827–835, Jul. 1994.

[2] K. A. C. de Macedo, R. Scheiber, and A. Moreira, "An autofocus approach for residual motion errors with application to airborne repeat-pass SAR interferometry," *IEEE Trans. Geosci. Remote Sens.*, vol. 46, no. 10, pp. 3151–3162, Oct. 2008.

[3] L. Yang, M. Xing, Y. Wang, L. Zhang, and Z. Bao, "Compensation for the NsRCM and phase error after polar format resampling for airborne spotlight SAR," *IEEE Geosci. Remote Sens. Lett.*, vol. 10, no. 1, pp. 165–169, Jan. 2013.

[4] F. H. Wong and T. S. Yeo, "New applications of nonlinear chirp scaling in SAR data processing," *IEEE Trans. Geosci. Remote Sens.*, vol. 39, no. 5, pp. 946–953, May 2001.

[5] X. Qiu, D. Hu, and C. Ding, "An improved NLCS algorithm with capability analysis for one-stationary BiSAR," *IEEE Trans. Geosci. Remote Sens.*, vol. 46, no. 10, pp. 3179–3186, Oct. 2008.

[6] G. Fornaro, "Trajectory deviations in airborne SAR: Analysis and compensation," *IEEE Trans. Aerosp. Electron. Syst.*, vol. 35, no. 3, pp. 997–1009, Jul. 1999.

[7] B. Rigling and R. Moses, "Motion measurement errors and autofocus in bistatic SAR," *IEEE Trans. Image Process.*, vol. 15, no. 4, pp. 1008–1016, Apr. 2006.

[8] D. G. Thompson, J. S. Bates, D. V. Arnold, and D. G. Long, "Extending the phase gradient autofocus algorithm for low-altitude stripmap mode SAR," in *Proc IGARSS*, Hamburg, Germany, Jul. 1999, pp. 564–566.

[9] W. Ye, T. S. Yeo, and Z. Bao, "Weighted least-squares estimation of phase errors for SAR/ISAR autofocus," *IEEE Trans. Geosci. Remote Sens.*, vol. 37, no. 5, pp. 2487–2494, Sep. 1999.